

RSC Advances

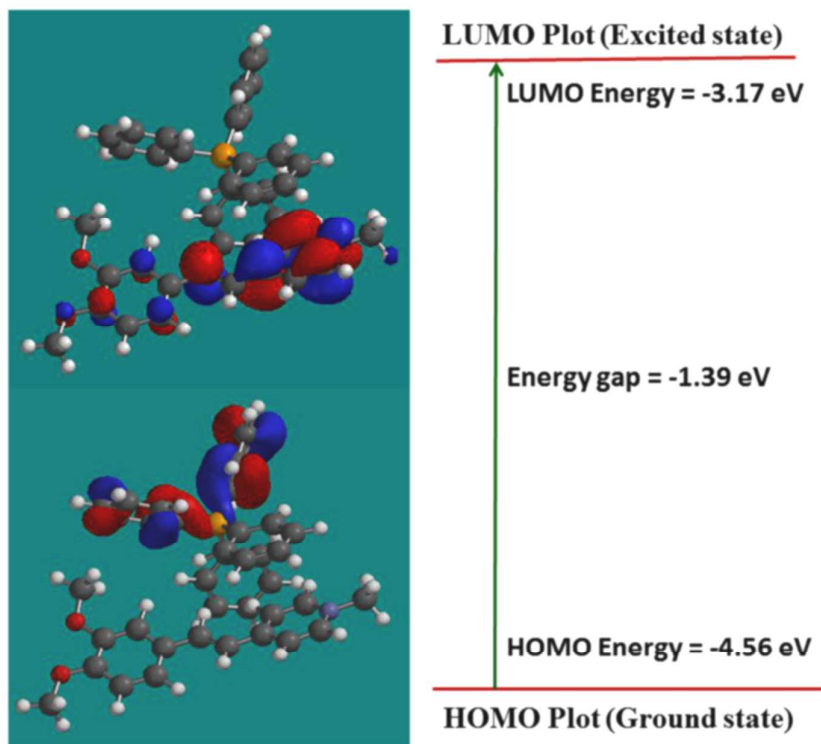


This is an *Accepted Manuscript*, which has been through the Royal Society of Chemistry peer review process and has been accepted for publication.

Accepted Manuscripts are published online shortly after acceptance, before technical editing, formatting and proof reading. Using this free service, authors can make their results available to the community, in citable form, before we publish the edited article. This *Accepted Manuscript* will be replaced by the edited, formatted and paginated article as soon as this is available.

You can find more information about *Accepted Manuscripts* in the [Information for Authors](#).

Please note that technical editing may introduce minor changes to the text and/or graphics, which may alter content. The journal's standard [Terms & Conditions](#) and the [Ethical guidelines](#) still apply. In no event shall the Royal Society of Chemistry be held responsible for any errors or omissions in this *Accepted Manuscript* or any consequences arising from the use of any information it contains.



Bulk crystal growth and Nonlinear optical characterization of stilbazolium derivative crystal: 4-[2-(3, 4-Dimethoxyphenyl) ethenyl]-1 methyl pyridinium tetraphenylborate (DSTPB) for NLO device fabrications

K. Senthil^{a,c}, S. Kalainathan^{a,*}, Fumio Hamada^b, Yoshihiko Kondo^c

^{a, a*}Centre for Crystal Growth, School of Advanced sciences, VIT University, Vellore - 632 014, India. Corresponding author: Phone: +91-416-2202350

E-mail Id: kalainathan@yahoo.com

^bDepartment of Applied Chemistry, Graduate School of Engineering & Resource Science, Akita University, 1-1 Tegatagakuen-cho Akita 010-8502, Japan

^cDepartment of Life Science, Graduate School of Engineering & Resource Science, Akita University, 1-1 Tegatagakuen-cho Akita 010-8502, Japan

Abstract

Search for highly efficient nonlinear optical (NLO) property of organic crystal with a high surface laser damage threshold (LDT) has become more demand in frontier areas of optical switching and communications applications. A single crystal of 4-[2-(3, 4-Dimethoxyphenyl) ethenyl]-1 methyl pyridinium tetraphenylborate (DSTPB), which is an organic material has been successfully synthesized in pure phase. Bulk single crystals were grown with dimensions of 28x11x6 mm³ using a slow evaporation method and report on the first in literature. The structure of the title crystal and its lattice parameter was confirmed by single-crystal X-ray diffraction studies and found that it crystallizes in the non-centrosymmetric space group Cc with monoclinic crystal system. The calculated HOMO and LUMO energies are showed that charge transfer takes place in the within the molecular structure, and they also indicate that NLO activity of the title crystal. It is Kurtz powder test showed large second harmonic generation (SHG) about 4.53 times that of KDP crystal and made it a suitable candidate for electro-optic applications. It also an exhibit good transparency (371nm–1100 nm) in the Visible and near infra-red spectral (NIR) ranges and is thermal stability was found to be up to 260 °C. It shows high laser-induced damage

threshold up to $4.3\text{GW}/\text{cm}^2$, which is greater than that of some known organic and inorganic NLO materials. Third-order nonlinear optical properties of title crystal were studied by single beam Z-scan technique at 632.8nm using He-Ne laser. It was found that they exhibit saturable absorption (SA) and self-focusing nature with large second-order hyperpolarizability (γ) 3.15×10^{-33} esu, which are mainly associated with electronic processes. The result indicates that they exhibit large third-order optical susceptibility compared some reported NLO crystals. The enhancement of these results second-order and third-order optical nonlinearity of DSTPB makes it a promising candidate for in the field of nonlinear optical devices.

Keywords

Organic crystal; FTIR; HOMO-LUMO analysis; Laser damage threshold; Second and third harmonic generation.

Introduction

The second-order nonlinear optical (NLO) materials containing organic chromophores are played a key role in constructing blocks for organic electro-optic OEO material.^{1,2} Research of nonlinear optical material containing pyridinium units has been proved to a good candidate for optoelectronic and photonics industries. In recent years, the design and synthesis of organic π -conjugated donor/acceptor materials have attracted tremendous attention because of their interesting applications in optical communication, optical computing, second harmonic devices, data storage systems, optical limiting, modern information technology, and so on.³⁻⁷ Among the organic and inorganic crystals, organic stilbazolium derivatives have attracted considerable attention due to their large second-order optical nonlinearity, modulation of laser reading, terahertz (THz) wave applications including THz detection and generation.⁸⁻¹² The origin reason for this is due to the presence of active

hydrogen bonds with π -conjugated system and Coulomb interactions between stilbazolium cation and counter anion.¹³⁻¹⁷ The experimental results are also proved the combination of large NLO response with a better mechanical, low dielectric constant, photochemical, and thermal stability. It is easy to modify the structure for the construction of integrated optical devices than the inorganic materials.¹⁸⁻²⁰ In the recent past, many stilbazolium derivatives have been widely investigated by different research groups using the same stilbazolium cation with counterion variations (aryl sulfonate anions) in order to expecting a new molecules with large NLO response which is based on Coulomb interactions. For example, DAST (4-N, N-dimethylamino-4'-N'-methyl-stilbazolium tosylate) with para-toluene sulfonate anion, DSNS (4-N, N-dimethylamino-4'-N'-methyl-stilbazolium 2-naphthalenesulfonate) with 2-naphthalenesulfonate anion has been first reported with extremely large nonlinearity.^{14,21} Over the last few decades, most of the research articles are focused mostly on second harmonic generation (SHG) of crystal.

However, there has been large the need of molecules with large third-order susceptibilities has been established to play the major role in all-optical switching/limiting devices, photonics and optoelectronics device applications.²²⁻²³ It has been recently reported that among the organic compounds stilbazolium derivatives yields high third-order NLO efficiency is mainly due to the presence of strong intramolecular charge transfer (ICT) transition.²⁴ For the first time, we present here the investigations on the bulk growth of DSTPB, spectral, HOMO-LUMO analysis, thermal stability, Vickers microhardness, dielectric properties, surface analysis, and photoconductivity studies. The structural relationship second-order [SHG] and third-order [THG] NLO properties of DSTPB have been investigated to realize the nonlinear optical properties by HOMO by LUMO analysis. The result indicates that the NLO activity is far larger than well-known KDP crystal.

2. Experimental Procedures

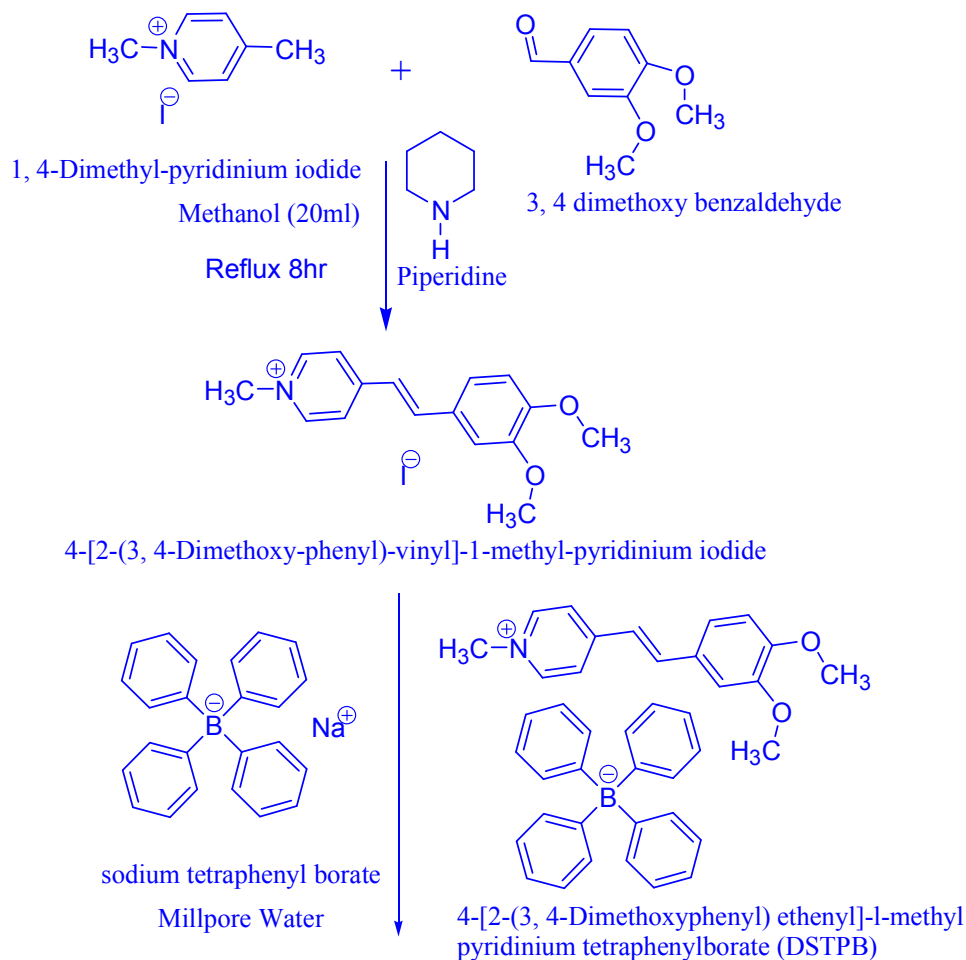
2.1. Material synthesis and Bulk crystal growth

Initially, analytical pure grade of iodomethane, 4-methylpyridine, 3,4-dimethoxybenzaldehyde, and sodium tetraphenylborate were purchased from Alfa Aesar and Sigma-Aldrich and used for synthesis of title material without further purification.

The title compound was synthesized by previously reported method (Scheme 1).²⁵ In the present synthesis process, the title crystal was prepared by two-step synthesis route. In the first step, 4-[2-(3,4-Dimethoxy-phenyl)-vinyl]-1-methyl-pyridinium iodide **1** which was synthesized by adding 1:1 molar ratio of 1,4-Dimethyl-pyridinium iodide, 3,4-dimethoxy benzaldehyde, and piperidine (few drops) in hot methanol (20ml). The resulting reaction mixture was refluxed for 8h. The resultant pale yellow precipitate which formed was filtered off and washed with diethyl ether and purified by repeated recrystallized from methanol. In the second step, the resultant purified compound **1** (electron attracting group-cation) was dissolved in deionized water (40ml) and mixed with a saturated aqueous solution of sodium tetraphenylborate (electron donating group-anion). Further, it was refluxed for 1 h at 80°C. The mixture immediately yielded pale yellow solid of 4-[2-(3,4-Dimethoxyphenyl) ethenyl]-1-methyl pyridinium tetraphenylborate (DSTPB) **2** when the solution was slow cooling to room temperature. The resulting DSTPB was washed with deionized water, and the purity was improved by successive recrystallization in methanol for several times.

The purified salt of DSTPB was dissolved in DMF at 40°C to form a saturated solution, and the solution has been stirred by using the motorized magnetic stirring device for 2h until to get a homogeneous solution. The resultant solution was filtered to 150ml beaker by using high-quality Whatmann filter paper. It was allowed to slow evaporation of the solvent at 40°C in a constant temperature water bath (accuracy of $\pm 0.01^\circ\text{C}$). The optical

qualities of DSTPB crystals were harvested with dimensions $28 \times 11 \times 6 \text{ mm}^3$ after a period of 45 days by macro defect free seed applied to the saturated solution as shown in Fig. 1a.



3. Results and Discussions

3.1. Single crystal and powder X-ray diffraction analyzes

The suitable size of grown single crystal was selected and subjected to single crystal XRD analysis by using Bruker Kappa APEX II diffractometer (MoK α $\lambda=0.71073\text{\AA}$ radiation). It reveals that the grown crystal crystallize in the monoclinic crystallographic system has non-centrosymmetric space group Cc. The cell parameter of DSTPB crystal has been obtained that $a=11.2979(2)\text{\AA}$, $b=16.988(2)\text{\AA}$, $c=17.2547(2)\text{\AA}$ and $\beta=100.232(10)\text{\AA}$.

The volume of the crystal system is 3254 (\AA)^3 . The obtained cell parameter values are similar to the reported values (CCDC-137966).²⁵ and thus confirm the grown title crystal. The crystal structure and packing fraction of DSTPB are shown in Fig. S1 and S2, respectively.

The grown crystals were finely powdered and subjected to powder X-ray diffraction analysis using BRUKER X-Ray diffractometer with the CuK α radiation ($\lambda=1.540598 \text{ \AA}$). The XRD profile reveals (Fig. S3) that well-defined sharp Bragg's peaks at specific 2θ angles and without detectable impurities. The obtained diffraction peaks were indexed by using Powder-X software package. The experimentally observed XRD peaks are matched closely with that of single crystal XRD pattern and shown in Fig. S3. Thus, the XRD analysis confirms the good crystallinity nature and purity of the title compound.

Knowledge of the growth morphology of DSTPB was generated and indexed by using a single crystal XRD data (CIF format) was given as input to the WinXMorph software program.²⁶ The indexed morphology of DSTPB is shown in Fig.1b. It was found that the (0 0 1) is the most prominent plane, and the faster growth rate is elongated along with crystallographic a and b direction compared to c-axes.

3.2. HOMO and LUMO studies

In order to know the relationship between frontier molecular orbitals energy gap (HOMO and LUMO) and nonlinear response of DSTPB crystal, the frontier molecular orbitals energy gap was calculated by using Spartan'10 V1.0.1 program.²⁷ The frontier molecular orbitals energy gap (HOMO and LUMO) is very important to characterize the optical polarizability, electrical, the nature of reactivity, kinetic stability of the molecule as well as in quantum chemistry.²⁸ The HOMO energy represents the ability to electron donating nature, and LUMO energy characterizes the ability to obtain an electron.

A molecule with small energy gap is more polarizable, which encourages the most active NLO properties of the system and also defined as the soft nature of the molecule.²⁹ As seen from Fig. S4, the HOMO orbitals are only localized on the two of phenyl rings in the tetraphenylborate (counter anion) while LUMO orbitals are located over the stilbazolium cation except in methyl groups and a counter anion. The calculated energy gap (energy gap = HOMO-LUMO) and dipole moment values are -1.39eV and 19.3D respectively. The low values of the energy gap and higher value of dipole moment implies that the molecular charge transfer is taking place within the molecule. This influence more polarizability of the structure and it is directly related to the NLO efficiency of the DSTPB structure.

3.3. Molecular electrostatic potential surface

The molecular electrostatic potential (MEP) surface diagram is used to know the reactive behaviour, electron density distributions and nucleophilic and electrophilic attack of the molecule in term of color grading.³⁰⁻³² The negative region is for nucleophilic site whereas the positive region is for potential electrophilic centres as shown in Fig. 2. The color line of MEP is found to in the range between 243.5a.u. (deepest red) and -244.2a.u. (deepest blue) for the title compound. It is clearly showed that (Fig.2) positive region are clearly located on the one of phenyl groups counter anion and methoxy groups in stilbazolium cation. The positive region covers only on the pyridinium ring in the stilbazolium cation whereas predominance of the green region (zero potential) in the MEP surfaces explains the potential halfway between the counter anion and stilbazolium cation. Thus, the MEP confirms the existence of intramolecular interactions.

3.4. FT-IR spectral studies

In order to confirm the presence of various vibrational motions of the functional groups in the grown crystal, FT-IR transmittance spectra have been recorded in the wavenumber range 4000–400 cm^{-1} using SHIMADZU IRAFFINITY spectrometer. Powder

of the title crystal (3mg) was mixed thoroughly with dried KBr (300mg) and made as pellets, and it was subjected for FTIR analysis. Fig.3. shows the FT-IR spectra of the title crystal. The absorption peak at 3443 cm^{-1} is corresponding to the H-O bond stretches in H_2O , which may be the moisture absorption from the atmosphere. The aromatic ring exhibits multiple bands in the region $3100\text{--}3000\text{ cm}^{-1}$ due to the C-H in-plane and C-H out of plane bending vibrations.³³ The band at 2831 cm^{-1} is assigned to the methoxy C-H stretching mode vibrations.³⁴ The peak seen at 2964 cm^{-1} assigned to C-H stretching vibrations of the methyl group (N-CH_3) in pyridine ring. The aromatic C=C stretching vibrations and in-plane stretching frequency of π -conjugated stilbazolium chromophore C-C=C-C (DSTPB structure) was established by the presence of peaks appear about 1647 cm^{-1} and 1579 cm^{-1} . It is responsible for an electron delocalization between the strong electron donor and electron acceptor of DSTPB. The peak observed at 1595 cm^{-1} is corresponding to the olefinic C-C stretching vibrations. The asymmetric bending vibrations of the methyl group (O-CH_3) are usually, found in the region $1465\text{--}1440\text{ cm}^{-1}$.³⁵ The observed peaks in the region $1150\text{--}850\text{ cm}^{-1}$ can be attributed to the skeletal vibrations of C-C and C-N bond. Thus, all the necessary strong NLO active vibrational modes functional groups of DSTPB crystal were confirmed from the characterization results.

3.5. UV–Vis–NIR Spectral Analysis

Optical transmittance ranges of single crystals are important factors for nonlinear optical applications because an optical material can be of practical device use only if it has lesser absorption of light in the Vis–NIR region.³⁶ To find the transmission window, the UV–Vis–NIR absorption spectrum (Fig. 4a) of DSTPB was measured with a ELICO SL 218 double beam UV–Vis–NIR spectrometer in the wavelength range between 190 and 1100 nm. It is clear from Fig. 4a, the title crystal possessing wider transparency in the Vis–NIR region. The optical absorption was found to be at 278 and 396nm. The lower cutoff of a wavelength

at 258nm is due to the n- π electronic transitions, and another one major peak at 398 nm corresponds to the π - π^* electronic transitions through extended conjugated system (stilbazolium chromophore). Hence, it can be a potential candidate for optoelectronic and NLO applications.³⁷

3.6. Photoluminescence studies

Fig. 4b. shows the photoluminescence (PL) spectrum of DSTPB was recorded from 340-650nm by using anF-7000 FL spectrophotometer at room temperature. The spectrum exhibits stable, strong emission peak at 471nm when excited by Uv-Vis light at 389 nm. The maximum intensity at 471nm (2.63 eV) is attributed to the π - π^* electronic transition between the donor ($C_{16}H_{18}NO_2^+$) and acceptor groups ($C_{24}H_{20}B^-$) through stilbazolium chromophore. It caused luminescence characteristic nature of DSTPB. Absence of any other emission peak in the measured region confirms good degree of crystallinity and structural perfection of DSTPB.³⁸ Hence, the resultant emission peak shows that material has blue emission, and it is more suitable for tunable laser system and optoelectronic devices.^{39, 40}

3.7. Thermo-gravimetric and Differential Thermal Analysis

TGA and DTA analysis is one of the most important for NLO material to throw light irritation on the thermal behaviour of the substance.⁴¹ To analyze the melting point, thermal behaviour, and the decomposition point of the DSTPB crystal has been obtained by using an NETZSCH STA 409 F3 thermal analyzer and the results shown in Fig. S5. The TG-DTA curves for DSTPB were recorded for the range of temperature from 30 to 550°C at a heating rate of 10°C/min under flowing N₂ gas. The initial pure sample of weight 3.196mg was used for the analysis. The TGA trace shows the first weight loss is 3.46% over the temperature range 35 to 245°C, which illustrates the loss of physically adsorbed moisture and volatile solvents during the crystallization. This is followed by two major weight losses occurred in the TGA. The first step is associated with a major weight loss of about 63.99% between 245

and 315°C, and another weight loss corresponds to 26.92% up to 550°C. These resultant weight losses are indicated decomposition of DSTPB and get volatilization gradually. Finally, TGA shows the final residual mass of weight is only 5.63% after heating to 550°C. In the DTA trace, one endothermic peak was found to be at 260°C, which is assigned to the melting point of DSTPB. It has followed by stepwise broad decomposition peak at 315°C occurs between 245 and 550°C. These endotherms are associated with decomposition of DSTPB crystal structure. A similar observation has also been well with the TGA trace. Hence, on the basis of this analysis concluded that the material for NLO applications is up to its melting because of there is no exothermic or endothermic peaks up to the melting point.

3.8. Microhardness Studies

The microhardness of a crystalline solid mainly depends on the crystal structure, the number of bonds per unit volume and composition of the crystalline solids.⁴² Microhardness of a crystal is strongly influenced by various parameters such as interatomic spacing lattice energy, Debye temperature and heat of formation.^{43,44} Calculation of mechanical properties of materials such as resistance, fracture behavior, brittleness index, yield strength, elastic constants, and temperature of cracking are very important in device fabrications.⁴⁵ The well-polished prominent plane (1 0 0) surface of DSTPB crystal was subjected to microhardness studies at room temperature using a MH-112 Vicker's hardness tester (Mututoyo MH 112, Japan) fitted with a diamond pyramidal indenter. In the present investigation, the applied load P was varied between 10–100g and indentations time is allowed to intent at 10s for all indentations. The average of two diagonal lengths (d) of the indentation mark was measured for each load by using with the help of calibrated micrometer attached to a metallographic microscope. The microhardness number (H_v) value was calculated from the following formula.⁴⁶

$$H_v = \frac{1.8544 \times P}{d^2} \left(\frac{\text{kg}}{\text{mm}^2} \right) \quad (1)$$

Where P is the applied load in kg and d is the average diagonal length of indentation impression in μm , and 1.8544 is a constant of a geometrical factor for the diamond pyramid indenter. Fig. S6. shows the variation of H_v with applied load. From this graph, it is very clear that the grown DSTPB crystal exhibits reverse indentation size effect (ISE). It means that, increase in H_v with an increasing applied load (P) in the low load region.⁴⁷⁻⁴⁹ The increase of H_v is purely due to the work hardening of the surface layers, and ISE may be attributed to the generation of cracks around the indentation.^{47, 50} The value of the Meyer index or the work hardening coefficient (n) was calculated from Fig. S7 a, the least-squares fitting method.⁵¹ In this study, Meyer index number is estimated to be 2.5. It is in good agreement with Onitsch concept that if n is >2 H_v value should increase with the increase in load P and reverse ISE behavior.^{52, 53} Thus, the calculated value of Meyer index number is suggesting that DSTPB belongs to be a softer organic materials category. From the hardness value, the yield strengths of the title crystal can be calculated using the following relation

$$\sigma_y = \frac{H_v}{2.9} [1 - (n - 2)] \left(\frac{12.5(n - 2)}{1 - (n - 2)} \right)^{n-2} \quad (2)$$

Fig. S7 b. shows the dependent yield strength as a function of applied loads 10 to 100 g. The stiffness constant gives an idea about the nature of bonding between neighboring atoms.⁵⁴ The elastic stiffness constant (C_{11}) can be calculated for loads from 10 to 100g (Fig. S7 c) by using Wooster's empirical expression as

$$C_{11} = (H_v)^{7/4} \quad (3)$$

Table 1 presented the calculated yield strength and stiffness constant for different loads.

3.8.1. Analysis of Hays-Kendall approach

According to Hays-Kendall approach⁵⁵ there is a minimum load W to initiate plastic deformation and the load dependence of hardness of grown crystal has been calculated using the relation $P=W+A_1d^2$, where W and A_1 are the minimum loads to initiate plastic deformation and load-independent constant and the exponent $n=2$. The values of W and A_1 (slope value) can be estimated by plotting the load (load range 10 to 100g) vs. d^2 (Fig. S7 d). The value of plastic deformation 'W' is the intercept value along the load axis (Y-axis). It is defined as the resistance pressure for the duration of indentation process, and it should be smaller than the applied load P .⁵⁶ The corrected hardness H_o (Table S1) for title crystal can be estimated using the formula $H_o = 1854 \times A_1$. Thus, the DSTPB crystal has a hardness value of 27 kg/mm^2 at 100g, which favors the grown DSTPB, can be a good candidate for NLO applications. It is significantly higher than to some NLO crystals such as urea ($6.5\text{-}11 \text{ kg/mm}^2$) and N-methyl urea ($12\text{-}19 \text{ kg/mm}^2$).⁵⁷ The good mechanical property defines the strong intramolecular interactions of title crystal.

3.9. Chemical Etching Studies

The nonlinear efficiency of devices mainly depends on the quality of the grown crystals because the imperfections occur during growth result in the distortion of the optical beam. For good performance of optical devices, crystals free from defects and light scattering are required.⁵⁸ The utility of NLO crystal depends on its surface quality because of laser damage threshold of the NLO crystals decreases with increasing defects in crystals.⁵⁹ The etching studies were carried on the as-grown crystal with crack-free surfaces is completely immersed in N, N-dimethylformamide as the etchant for an etching time of 20-40s. Then the etched surfaces were cleaned by using tissue paper, and their microstructures were examined using an optical microscope (Carl Zeiss optical microscope with a 50x magnification). Fig. S8 a. Shows the surface micrograph of the as-grown crystal. The

microstructure of the etched crystal surface for etching time 20-40s is shown in Fig. S8 b and S8 c). It is observed that size of etch pits decreases with the increase of etching time. These results suggest that the grown crystal has rectangular type growth mechanism with less dislocation reveals better crystalline perfection.

3.10. Laser-Induced Damage Threshold Studies

The operation of NLO devices depends not only on the linear and nonlinear optical (NLO) properties but also must be the ability to withstand high-power lasers intensities source. Because of the second harmonic conversion efficiency is proportional to the density of incident beam intensities.^{60,61} Hence, newly discovered NLO materials with high optical surface damage tolerance (by high-power lasers) become extremely important in the performance of nonlinear optical (NLO) and optoelectronic device applications.^{62,63} For this measurement, a Q-switched Nd: YAG (1064 nm radiation) pulsed laser was used, and the pulse width are 10ns with 10 Hz repetition rate with operating in transverse TM00 mode. During laser irradiation, damage of the surface can be determined by the visual formation damage and the input laser energy density was recorded by a power meter (model no: EPM 2000). The damaged spot was measured using Carl Zeiss optical microscope with a 50x magnification. The laser damage threshold of the grown crystal was evaluated by the following relation.⁶⁴

$$I = \frac{E}{\tau A} \quad (4)$$

Where I is the energy density required to cause damage, E is the input energy measured in mJ, τ is the pulse Width, A is the area of the laser spot. Thus, the estimated surface damage threshold value of DSTPB crystal is found to be 4.3GW/cm². It is higher than that of well-known KDP crystal (0.2 GW/cm²) and urea (1.5 GW/cm²).⁶⁵

3.11. Dielectric studies

3.11.1. Dielectric constant and dielectric loss measurements

Dielectric properties are highly related to the quality information of materials.⁶⁶ The selected grown crystals were cut and polished to obtain about 2 mm thickness. It was subjected to dielectric studied at room temperature using HIOKI 3532-50 LCR HITESTER meter in the frequency region 50Hz -5 MHz. The opposite surface of the crystals was coated with high-grade silver paste and was placed between two copper electrodes, and thus uniform electrical contact was formed on the crystal surface. The dielectric constant (ϵ_r) and dielectric loss ($\tan \delta$) were calculated using the standard relations.⁶⁷ From the results (Fig.5a and 5b), a variation of dielectric constant and dielectric loss was found to a high value at low frequencies region. Further, it is decreased with the increase of frequencies and attain almost constant at higher frequencies region. Hence, it increases the material for the fabrication of NLO devices and electro-optic applications.⁶⁸⁻⁷⁰ The large value of both dielectric constant and dielectric loss at low-frequency region can be explained on the basis of the contribution of space charge polarization.⁷¹ In general, the magnitude of dielectric constant and dielectric loss purely depends on the chemical structure (purity), electric field, the perfection of the crystal also the temperature.⁷²

3.11.2. DSTPB crystal based on single crystal XRD

Solid state parameters are important to estimate the electronic polarizability of the material and to evaluating its SHG efficiency. The SHG efficiency depends upon the electronic polarizability of the medium. To interpreting SHG efficiency, the high frequency dielectric constant value of DSTPB is used as input to estimate the electronic properties like valence electron plasma energy, Penn gap, Fermi energy and electronic polarizability. From the single XRD studies, the molecular weight of DSTPB is $M = 575.5\text{g/mole}$ and density $\rho = 1.172\text{gcm}^{-3}$. The value of dielectric constant at 1MHz is calculated to be $\epsilon_r = 185$.

The total number of valence electrons of DSTPB is $Z = 218$. From this data, the valence electron plasma energy $\hbar\omega_p$ can be calculated using standard relation.⁷³

$$\hbar\omega_p = 28.8 \left(\frac{Z\rho}{M} \right)^{\frac{1}{2}} \quad (5)$$

According to the Penn model⁷⁴, the average Penn gap (E_p) and Fermi energy (E_F)⁷⁵ for DSTPB are calculated using the relation

$$E_p = \frac{\hbar\omega_p}{(\epsilon_\infty - 1)^{1/2}} \quad (6)$$

$$E_F = 0.2948(\hbar\omega_p)^{1/2} \quad (7)$$

Then, we obtained electronic polarizability (α) of the title crystal using the relation⁷⁶

$$\alpha = \left[\frac{(\hbar\omega_p)^2 S_0}{(\hbar\omega_p)^2 S_0 + 3E_p^2} \right] \times \frac{M}{\rho} \times 0.396 \times 10^{-24} \text{ cm}^3 \quad (8)$$

Where S_0 is a constant which can be obtained by

$$S_0 = 1 - \left[\frac{E_p}{4E_F} \right] + \frac{1}{3} \left[\frac{E_p}{4E_F} \right]^2 \quad (9)$$

The obtained value of polarizability α agrees well with that of Clausius–Mossottiquation which is given by

$$\alpha = \frac{3M}{4\pi N_a \rho} \left(\frac{\epsilon_\infty - 1}{\epsilon_\infty + 2} \right) \quad (10)$$

where N_a is Avogadro number. These solid state parameters values are compared with those of standard material KDP and listed in Table S2. From the table, the polarizability of DSTPB is found to be more than that of KDP.⁷⁷ This result is in good agreement with the Kurtz and

Perry powder technique. Thus, the result is concluded that SHG efficiency depends on the polarizability of the medium.⁷⁸

3.12. Second harmonic generation efficiency measurements

It is worthy to study the SHG efficiency DSTPB crystal by the Kurtz and Perry powder technique.⁷⁹ and the effectiveness of the title compound compared with well-known SHG microcrystalline powder of KDP. In the present investigation, the crystal (DSTPB and KDP) was fine powdered with uniform particle size and subjected to powder XRD studies. The particle size was determined by using the Scherer equation and was found to be 125-150 μm . When a fundamental laser beam of 1064 nm from a Q-switched Nd: YAG laser with 8 ns pulse width and 10 Hz repetition rate were normally exposed on the pre-packed microcapillary tube. The frequency conversion was confirmed by the emission of green radiation (second harmonic signal (SHG) $\lambda=532$ nm) with an output pulse are 8.8 mV and 39.9 mV for DSTPB and KDP respectively. The SHG responses mainly depend on the particle size, field-gain coefficient, the power of the fundamental beam and minimum beam waist.⁸⁰ Comparing the SHG conversion efficiency, the title compound was found to be about 4.53 times that of KDP crystal. Thus, the good SHG efficiency suggests that the title compound can be a potential candidate for frequency conversion applications.

3.13. Z-scan measurements

The third-order nonlinear optical properties of DSTPB was investigated by the standard Z-scan technique.⁸¹ It is widely used to evaluate both the nonlinear absorption and nonlinear index (n_2) of the material along with the sign of nonlinearity. In this experiment was performed with He-Ne laser at 632.8nm as the excitation source with a beam diameter 0.5 mm. The output of the laser beam was focused with a Gaussian filter to get the Gaussian intensity profile, which was focused by a 30mm focal length lens. The beam waist ω_0 of Gaussian beam at the focal point is measured to be 12.25 μm . It is known that the thickness of

the sample is very important to minimize the phase transition in Z-Scan experiment. For this technique the sample thickness of 0.65mm was used. It is less than the Rayleigh diffraction length ($L < K = ZR$, where L is the thickness of crystal, and ZR is corresponding to the Rayleigh diffraction length of the Gaussian beam). The Rayleigh length was calculated about 0.72 mm using the formula $ZR = \pi \omega_0^2 / \lambda$ (λ is the wavelength).⁸² Hence, its thickness condition could be satisfied with a thin medium for this measurement. The crystal is translated in the direction of negative $-Z$ to positive $+Z$ axis (laser beam direction) under the computer-controlled translation stage. The amplitude of the phase shift was monitored by the change in the transmitted intensity through a small aperture with respect to the sample position (closed aperture method) using a digital power meter. The variations of transmitted intensity completely depend on the aperture size since the large aperture size will reduce the variations in transmittance intensity. For an open aperture method, intensity dependent absorptions were collected directly in the detector by placing lens in front of the detector and without placing an aperture at the detector in order to resolve the nonlinear refraction (NLR) and nonlinear absorption (NLA). As the crystalline, sample exposed to the focal plane the intensity of the laser beam decreases or increases directly depends on the material refractive index and its absorption nature. Fig. 6a and 6b depict the closed and open aperture Z- scan curves of title crystal. The open aperture scan method indicates that absence of reverse saturation absorption (RSA) with the enhanced transmission towards the focal point, which concludes the strong saturation of absorption (SA) process in DSTPB. It is a necessary parameter of the material to finds application in the laser applications such as laser pulse compression, laser pulse narrowing, and optical switching applications.⁸³⁻⁸⁵ This type of a saturation process (SA) at the focal point is known as ground state absorption than the absorption of the excited state. In the closed aperture data, the valley and peak configuration clearly suggest that the title crystal has a positive sign of third-order nonlinear refractive

index, which reveals the self-focusing effect. Complete experimental setup for Z-scan measurement can be found in our earlier work.^{86,87}

From the closed aperture Z-scan data, the difference between the normalized valley and peak transmittances (ΔT_{p-v}), as seen in Fig. 6b can be obtained using the relation^{81,88-89}

$$\Delta T_{p-v} = 0.406(1-S)^{0.25} |\Delta\Phi_0| \quad (11)$$

where S is the linear transmittance of the aperture in the absence of a sample which is obtained the following relation⁸⁵

$$S = 1 - \exp\left(\frac{-2r_a^2}{\varepsilon_a^2}\right) \quad (12)$$

where r_a is the radius of the aperture and ω_a is the beam radius at the aperture. The third-order nonlinear refractive index (n_2) of the grown crystal was calculated using closed aperture data, and it is given by

$$n_2 = \frac{\Delta\Phi_0}{KI_0L_{\text{eff}}} \quad (13)$$

where K is the wave vector ($K=9.924 \times 10^6 \text{ m}^{-1}$), λ is the wavelength of the laser and I_0 ($I_0=26.50 \text{ MW/m}^2$) is the intensity of the laser beam at the focal point ($Z=0$). The effective thickness of the grown crystal can be estimated as $L_{\text{eff}} = [1 - \exp(-\alpha L)] / \alpha$, where L is the thickness of the crystal and α is the linear absorption coefficient. The nonlinear absorption coefficient (β) can be estimated from the open aperture Z-scan data. The third-order nonlinear absorption coefficient (β) can be determined using open aperture data by the following formula⁸¹

$$\beta = \frac{2\sqrt{2}\Delta T}{I_0L_{\text{eff}}} \quad (14)$$

where ΔT is the peak value of the open aperture Z-scan curve. The obtained third-order nonlinear refractive index n_2 and nonlinear absorption coefficient are $7.85 \times 10^{-10} \text{m}^2/\text{W}$ and $1.02 \times 10^{-3} \text{m}/\text{W}$, respectively. It can be used to determine the real and imaginary parts of the third-order nonlinear optical susceptibility by the following formula.⁹⁰⁻⁹¹

$$\text{Re } \chi^{(3)}(\text{esu}) = \frac{10^{-4}(\epsilon_0 C^2 n_0^2 n_2)}{\pi} \left(\frac{\text{cm}^2}{\text{W}} \right) \quad (15)$$

$$\text{Im } \chi^{(3)}(\text{esu}) = \frac{10^{-2}(\epsilon_0 C^2 n_0 \lambda \beta)}{4\pi^2} \left(\frac{\text{cm}^2}{\text{W}} \right) \quad (16)$$

where ϵ_0 is the vacuum permittivity ($8.8518 \times 10^{-12} \text{F/m}$), n_0 is the linear refractive index of the crystal. The effective value of the third-order nonlinear optical susceptibility $\chi^{(3)}$ and the molecular second hyperpolarizability of the crystal can be calculated through the following expressions is given as

$$|\chi^{(3)}| = \left[(\text{Re}(\chi^{(3)}))^2 + (\text{Im}(\chi^{(3)}))^2 \right]^{1/2} \quad (17)$$

$$\text{Re}[\gamma] = \frac{\text{Re}[\chi^{(3)}]}{Nf^4} \quad (18)$$

where f is the local-field correction factor, and N is the number of molecule per unit volume in cm^{-3}

$$f = \frac{(n_0^2 + 2)}{3} \quad (19)$$

In order to know the suitability of grown crystal for all-optical switching device applications, the two figure of merit $W = n_2 I / \alpha \lambda$, $T = \beta \lambda / n_2$ was estimated for the title crystal based on the obtained third-order NLO parameter.⁹² For all-optical switching applications, the value of $W \gg 1$ and $T \ll 1$ is needed. So the calculated value of W is 1.81 and T is 15.53, which is way short for the requirement of all-optical switching device applications. However, it is a basic

requirement in laser Q-switching, laser mode-locking, and optical bistability field because of its strong saturation absorption (SA) properties.⁹³ The calculated third-order nonlinear optical parameters such as nonlinear absorption coefficient β , nonlinear refractive index n_2 , third-order nonlinear susceptibility $\chi^{(3)}$, second-order hyperpolarizabilities of the title crystal were tabulated in Table 2. The large value of $\chi^{(3)}$ can be attributed to the electron density transfer (donor to acceptor) within the molecular system.⁹⁴ Therefore, the polarization of π -conjugated electrons will be high in the molecular system and which contribute to the large value of $\chi^{(3)}$ and γ for the DSTPB crystal. The large third-order nonlinear property of DSTPB is compared with those of some organic NLO materials are tabulated in Table 3. Thus, the obtained results imply that the title crystal can be a good candidate for third-order NLO applications.

3.13. Photoconductivity study

Photoconductivity measurements were studied on the polished surface of the grown crystal using a Keithley 485 picoammeter at room temperature. Two thin copper wire were fixed at spacing of about 0.3cm by using of silver paint in order to give a good electrical contact. Then the sample was connected in series with a DC power supply and a picoammeter. For measuring the dark current, the DC supply was applied from 0 to 30V in steps of 2V, and the corresponding dark current was noted in the dark atmosphere. The same sample was exposed to the radiation with the help of a convex lens to measure the photocurrent using a halogen lamp (100 W) containing tungsten filament and iodine vapour. Then the corresponding photocurrent was noted for the same range of the applied field. Fig. S9 shows an increase in both the dark and photocurrent of the title crystal linearly with applied voltage. However, the dark current was seen to be less than the photocurrent, which defines the positive photoconductive property of title crystal. This phenomenon is due the absorption and excitation of charge carries when the illumination of radiation.^{97, 98}

This characteristic of photocurrent is actually played a key role in guided weapons, photodetection and Ultraviolet (UV) and Infrared (IR) detector applications.^{99, 101}

4. Conclusion

Bulk single crystal of DSTPB has been synthesized and grown by the slow evaporation method and characterized for its large NLO property. The lattice parameter was confirmed by single crystal XRD analysis. Various vibrational modes of functional groups present in the crystal established through FT-IR analysis. The grown crystal has the wide transparency nature in the Vis-NIR spectral range, which makes these crystals potentially active material for non-linear optical device applications. Luminescence assessment indicates strong emission of blue radiations around 471, and it may be used for the light emitting diode (LED) applications. The TG/DTA study shows that the crystal possesses good thermal stability up to 260°C. Mechanical studies reveal reverse indentation size effect (RISE) and crack develop for load above 100g. The work hardening coefficient was found to be 2.5, and yield strength (σ_y) and elastic stiffness constant (C_{11}) were calculated. The dielectric constant of the DSTPB signifying that the crystal is possessed excellent optical quality with defect-free nature. The grown crystal has superior laser damage threshold (4.3 GW/cm²) at 1064 nm wavelength of Nd: YAG laser and compared with some NLO materials. The etching study of DSTPB crystals reveals the layers type etch pattern. The powder SHG efficiency was found to be 4.53 times than that of KDP crystal. The third-order nonlinear optical study of DSTPB crystal reveals that the strong saturation absorption and positive sign of nonlinear refractive index (n_2). These results imply that the title crystal can be a used for third-order NLO applications. The obtained all the above results suggest that the grown is considered for the devices fabrication of optical limiting and photonic devices in the future.

Acknowledgements

The authors are thanking Defence Research and Development Organisation (DRDO), Government of India, for financial assistance to execute this research work and VIT University management for their help, constant support and scientific research facilities.

References

1. Feng gang Liu, Yuhui Yang, Shengyu Cong, Haoran Wang, Maolin Zhang, Shuhui Bo, Jialei Liu, Zhen Zhen, Xinhou Liua and Ling Qiu, *RSC Adv.*, 2014, 4, 52991
2. Q. Q. Li, C. G. Lu, J. Zhu, E. Fu, C. Zhong, S. Y. Li, Y. P. Cui, J. G. Qin and Z. Li, *J. Phys. Chem. B*, 2008, 112, 4545–4551.
3. S. R. Marder, B. Kippelen, Jen AK-Y, N. Peyghambarian, *Nature*, 1997, 388, 845.
4. H. Ma, Jen AK-Y, L. R. Dalton, *Adv Mater.*, 2002, 14, 1339.
5. N.B. Singh, T. Henningsen, E.P.A. Metz, R. Hamacher, E. Cumberledge, R. H. Hopkins, *Mater. Lett.*, 1991,12, 270–275.
6. W. Wu, R. Tang, Q. Li and Z. Li, *Chem. Soc. Rev.*, 2015, 44, 3997.
7. Z. Li, Q. Li and J. Qin, *Polym. Chem.*, 2011, 2, 2723.
8. G. Zhuo, X. Wang, D. Wang, C. Wang, Z. Shao, Q. Fang. M. Jiang, *Opt. Commun.*, 2001, 190, 345.
9. N. Nakanishi, H. Matsuda, S. Okada, M. Kato, *Proc. MRS Int. Mtg. Adv. Mater.*,1989,1, 97.
10. Z. Yang, L. Mutter, M. Stillhart, B. Ruiz, S. Aravazhi, M. Jazbinsek, A. Schneider, V. Gramlich, P. Gunter, *Adv. Funct. Mater.*, 2007, 17, 2018.

11. T. Matsukawa, Y. Takahashi, R. Miyabara, H. Koga, H. Umezawa, M. Kawayama, S. Yoshimura, M. Okada, Y. Tonouchi, Y. Kitaoka, T. Mori, Sasaki, *J. Cryst. Growth.*, 2009,311, 568.
12. T. Matsukawa, T. Notake, K. Nawata, S. Inada, S. Okada, H. Minamide, *Opt. Mater.*, 2014,36, 1995-1999.
13. X.M. Duan, H. Konami, S.Okada, H. Oikawa, H. Matsuda, H. Nakanishi, *J. Phys.Chem.*, 1996,100, 17780.
14. S.R. Marder, J.W .Perry, W.P. Schaefer, *Science*. 1989, 245, 626.
15. P.J. Kim, J.H.Jeong, M. Jazbinsek, S.J. Kwon, H. Yun, J.T. Kim, Y.S. Lee, L.H. Baek, F. Rotermund, P. Günter, O. P. Kwon, *CrystEngComm.*, 2011,13, 444.
16. F. Pan, M.S. Wong, Ch. Bosshard, P. Gunter, *Adv. Mater.*,1996, 8, 592.
17. J. Ogawa, S. Okada, Z. Glavcheva, H. Nakanishi, *J. Cryst. Growth.*, 310 (2008) 836.
18. H. Adachi, Y. Takahashi, J. Yabuzaki, Y. Mori, T. Sasaki, *J. Cryst., Growth.*, 1999, 98, 568.
19. X. M. Duan, H. Konami, S. Okada, H. Oikawa, H. Matsuda, H. Nakanishi, *J. Phys. Chem.*, 1996,100, 17780.
20. B. J. Coe, J. A. Harris, A. K. Clays, G. Olbrechts, A. Persoons, J. T. Hupp, R. C. Johnson, S. J. Coles, M.B. Hursthouse, K. Nakatani, *Adv. Funct. Mater.*, 2002, 12, 110.
21. B. Ruiz, Y. Yang, V. Gramlich, M. Jazbinsek, P. Gunter, *J. Mater. Chem.*, 2006, 16, 2839.
22. J. H. Klein-Wiele, M. A. Bader, L. I. Bauer, S. Soria, P. Simon, G. Marowsky, *Synth. Met.*, 2002,127, 53–57.
23. D. Y. Wang, C. L. Zhan, Y. Cheng, Y, J. Li, Z. Z. Lu and Y. X. Nie, *Chem. Phys. Lett.*, 2003, 369, 621.

24. C. Zhan, Y. Li, D. Li, D. Wang, Y. Nie, *Opt. Mater.*, 2006, 28, 289.
25. De-chunzhang, Li-Qinge, Ttan-Zhu Zhang, Yan-Qtu Zhang, Kai-Bei Yu. *Acta Cryst. C55.*, 1999, 1938-1939.
26. W.J. Kaminsky, *J. Appl. Crystallogr.*, 2007, 40, 382.
27. I. Fleming, *Frontier Orbitals and Organic Chemical Reactions*, Wiley, London. 1976.
28. T. Karakurt, M. Dinçer, A.Çetin, M. Sekerci, *Spectrochim. Acta, Part A.*, 2010, 77, 189-198.
29. E. Selvakumar, G. Anandhababu, P. Ramasamy, Rajnikant, T. Uma Devi, R. Meenakshi, A. Chandramohan, *Spectrochim. Acta, Part A.* 2014, 124, 114-119.
30. E. Scrocco, J. Tomasi, *Adv. Quantum. Chem.*, 1978, 103, 115-121.
31. N. Okulik, A. H. Jubert, *Int. Electron. J. Mol. Des.*, 2005, 4, 17-21.
32. F. J. Luque, J. M. Lopez, M. Orozco, *Theor. Chem. Acc.*, 2000, 103, 343-345.
33. G. Varsanyi, *Vibrational Spectra of Benzene Derivatives*, Academic Press, New York. (1969).
34. D. L. Vein, N. B. Colthup, W. G. Fateley, J. G. Grasselli, *The Handbook of Infrared and Raman Characteristic Frequencies of Organic Molecules*, Academic Press, New York. (1991).
35. M. Silverstein, G. C. Basseler, C. Morill, *Spectrometric Identification of organic compounds* Wiley, New York. (1981).
36. V. Krishnakumar, R. J Xavier, *Spectrochim. Acta, Part A.*, 2005, 61, 1799-1809.
37. P. N. Prasad, Springer, Ser. Wave-Phenom. 9 (1989) 305-327.
38. S. Sudhahar, M. Krishna Kumar, B.N. Sornamurthy, R. Mohan Kumar, *Spectrochim. Acta, Part A.*, 2014, 118, 929-937.
39. M. A. F. M. Da Silva, I. C. S. Carvalho, N. Cella, H.N. Bordallo, L.P. Sosman, *Opt. Mater.*, 2013, 543-546.

40. J. X. Wang, S. S. Xie, H. J. Yuan, X. Q. Yan, D. F. Liu, Y. Gao, Z. P. Zhou, L. Song, L. F. Liu, X. W. Zhao, X.Y. Dou, W. Y. Zhou, G. Wang, *Solid State Commun.*, 2004, 131, 435–440.
41. R. Sankar, C. M. Raghavan, and R. Jayavel, *Cryst. Growth Des.*, 2007, 7.
42. K. K. Rao, D. B. Sirdeshmukh, *B mater sci.*, 1983, 5, 449–452.
43. J. Jiaghong Gong, *Mater Sci. Lett.*, 2000, 19, 515.
44. R. Uthrakumar, C. Vesta, C. Justin Raj, S. Krishnan, S. Jerome Das, *Curr. Appl. Phys.*, 2010, 10, 548 – 552.
45. Mott, B., Ed. Micro Indentation Hardness Testing; Butterworth: London. 1956.
46. Mott, B. W. Micro Indentation Hardness Testing; Butterworths: London. 1957.
47. T. S. Shyju, S. Anandhi, R. Gopalakrishnan, *CrystEngComm.*, 2012, 14, 1387–1396.
48. M. Shakir, V. Ganesh, M. A. Wahab, G. Bhagavannarayana, K. K. Rao, *Mater. Sci. Eng. B.*, 2010, 172, 9-14.
49. P. Mythili, T. Kanagasekaran, R. Gopalakrishnan, *Cryst. Res. Technol.* 2007, 42, 791.
50. J. Hernandez-Paredes, O. Daniel Glossman-Mitnik, H. Hernandez-Negrete, M.E. Esparza-Ponce, R. Alvarez, R. Rodriguez Mijangos, A. Duarte-Moller, *J. Phys. Chem. Solids.*, 2008, 69, 1974–1979.
51. S. Kalainathan, K. Jagannathan, *J. Cryst. Growth.*, 2008, 310, 2043–2049.
52. E. M. Onistch, *Mikroskopia.*, 1947, 2, 131.
53. K. Sangwal, A. Klos, *Cryst. Res. Technol.*, 2005, 40, 429-438.
54. J. Rani ChristhuDhas, Charles Bennet and F. D. Gnanam, *J. Cryst. Growth.*, 1994, 137, 295.
55. C. Hays, E. G. Kendall, *Metallography.* 1973, 6, 275.
56. K. K. Banwari Lal, P. N. Bamzai, B.W. Kotru, Wanklyn, *Mater Chem Phys.*, 2004, 85, 353-365.

57. E. E. A. Shepherd, J. N. Sherwood, G. S. Simpson, *J. Cryst. Growth.*, 1996, 167, 709.
58. M. Senthil Pandian, P. Ramasamy, Binay Kumar, *Mater. Res. Bull.*, 2012, 47, 1587–1597
59. R. Ramesh Babu, S. Kumaresan, N. Vijayan, M. Gunasekaran, R. Gopalakrishnan, P. Kannan, P. Ramasamy, *J. Cryst. Growth.*, 2003, 256, 387–392.
60. G. C. Bhar, A. K. Chaudhary, P. Kumbhakar, *Appl. Surf. Sci.*, 2000, 161, 155–162.
61. Z. Sun, G. Zhang, X. Wang, Z. Gao, X. Cheng, S. Zhang, D. Xu, *Cryst. Growth Des.*, 2009, 9, 3251–3259.
62. N.L. Boling, M.D. Crisp, G. Dube, *Appl. Opt.*, 1973, 12, 650–660.
63. G.H. Sun, G.H. Zhang, Z.H. Sun, X. Q. Wang, D. Xu, *Mater. Chem. Phys.*, 2011, 127, 265–270.
64. Z. Sun, G. Zhang, X. Wang, Z. Gao, X. Cheng, S. Zhang, D. Xu, *Cryst. Growth Des.* 2009, 9, 3251.
65. K. Ambujam, K. Rajarajan, S. Selvakumar, I. VethaPotheher, P. Ginson, P. Joseph, Sagayaraj. *J. Cryst. Growth.*, 2006, 286, 440–444.
66. C. Balarew, R. Duhlew, *J. Solid State Chem.*, 1984, 55, 1–6.
67. K. Sethuraman, R. Ramesh Babu, R. Gopalakrishnan, P. Ramasamy, *Cryst. Growth Des.*, 2008, 8.
68. P. Rajesh, P. Ramasamy, G. Bhagavannarayana, *J. Cryst. Growth*, 2009, 311, 4069.
69. M. Vimalana, T. Rajesh Kumar, S. Tamilselvan, P. Sagayaraj, C. K. Mahadevan, *Physica B.*, 2010, 405, 3907–3913.
70. C. Balarew, R. J. Duhlew, *Solid State Chem.*, 1984, 55, 1–6.
71. IshwarBhat, P. Mohan Rao, A.P. Ganesh Bhat, D.K. Avasthi, *Surf. Coat. Technol.*, 2002, 158, 725–728.
72. J. S. Pan, X.W. Zhang, *Acta Mater.*, 2006, 54, 1343–1348

73. J. D. Jackson, *Classical Electrodynamics*, Wiley Eastern. 1978, 321.
74. D. R. Penn, *Phys. Rev.*, 1962, 128, 2093–2097.
75. N. M. Ravindra, R. P. Bhardwaj, K. Sunil Kumar, V. K. Srivastava, *J. Infrared Phys.*, 1981, 21, 369-381.
76. N.M. Ravindra, V.K. Srivastava, *J. Infrared Phys.*, 1980, 20, 67–69.
77. P. Vasudevan, S. Sankar, D. Jayaraman, *Bull. Korean Chem. Soc.*, 2013, 34.
78. P. Vasudevan, S. Sankar, S. GokulRaj, *Optik.*, 2013, 124, 4155- 4158.
79. S.K. Kurtz, T. T. Perry, *J. Appl. Phys.*, 1968, 44, 455.
80. P. C. RajeshKumar, V. Ravindrachary, K. Janardhana, BojaPoojary. *J. Cryst. Growth.* 2012, 354, 182-187.
81. M. Sheik-Bahae, A.A.Said, E.W. Van Stryland, *Opt. Lett.*, 1989, 14, 955.
82. T. T. Jia, He, P. Li, Y. Mo, Y. Cui, *Opt. Laser Technol.*, 2008, 40, 936.
83. Xiang-Bing Sun, Yan-Ling Wang, QuanRen, Fu-jun Zhang, Yi Gao, Hong-Liang Yang, Lin Feng, Xin-Qiang Wang, DongXu, *Opt. Mater.*, 2007, 29, 1305-1309.
84. A. LittyIrimpan, Deepthy, Bindu Krishnan. L. M. Kukreja, V. P. N. Nampoori, P. Radhakrishnan, *Opt. Commun.*, 2008, 281, 2938–2943.
85. V.P.N. Nampoori, P. Radhakrishnan, *Opt. Commun.*, 2008, 281, 2938–2943.
86. K. Senthil, S. Kalainathan, A. Ruban Kumar, P.G. Aravindan, *RSC Adv.*, 2014, 4, 56112.
87. K. Senthil, S. Kalainathan, F. Hamada, M. Yamada, P.G. Aravindan, *Opt Mater.*, 2015, 46, 565–577.
88. E. W. Van Stryland, M. Sheik-Bahae, M.G. Kuzyk, C.W. Dirk, New York: Marcel Dekker, Inc., 1998, 655-692
89. T. Kanagasekaran, P. Mythili, P. Srinivasan, A.Y. Nooraldeen, P. K. Palanisamy, R. Gopalakrishnan, *Cryst. Growth Des.*, 2008, 8, 2335-2339.

90. C. Gayathri, A. Ramalingam, *Spectrochim. Acta, Part A.*, 2007, 68, 578-82.
91. T. Cassano, R. Tommasi, M. Ferrara, F. Babudri, G. M. Farinola and F. Naso, *Chem. Phys.*, 2001, 272, 111-118.
92. J. Sun, W. F. Guo, X.Q. Wang, G.H. Zhang, X. B. Sun, L. Y. Zhu, Q. Ren, D. Xu, *Opt Commun.*, 2007, 280, 183-187.
93. He-Liang Fan, QuanRen, Xin-Qiang Wang, Ting-Bin Li, Jing Sun, Guang-Hui Zhang, Dong Xu, Gang Yu, Zhi-HuaSun, *Natural Science.*, 2009, 1, 136-141.
94. Y. S. Zhou, E. B. Wang, J. Peng, J. Liu, C.W. Hu, R. D. Huang, X. You, *Polyhedron*.1999, 18, 1419-1423.
95. M. Krishna Kumar, S. Sudhahar, A. Silambarasan, B.M. Sornamurthy, R. Mohan Kumar, *Optik*, 2014, 125, 751–755
96. E.D. D'silva, G. Krishna Podagatlapalli, S. Venugopal Rao, S.M. Dharmaprakash, *Materials Research Bulletin* 47 (2012) 3552–3557
97. R. H. Bube, *Photoconductivity of solids*, Wiley Interscience, New York. (1981).
98. N.V. Joshi, *Photoconductivity*, Marcel Dekker, New York. (1990).
99. R. N. Jayaprakash, P. Kumaradass, *Orient. J. Chem.*, 2013, 29, 1409-1414.
100. R. H. Bube. *Photoconductivity of Solids* New York: Wiley Interscience (1960).
101. B. Milton Boaz, R. Samuel Selvaraj, K Senthil Kumar, S Jerome Das. *Indian J. Phys.* 2009, 83, 1647-1657.